Science Advances

Supplementary Materials for

UV-B radiation was the Devonian-Carboniferous boundary terrestrial extinction kill mechanism

John E. A. Marshall*, Jon Lakin, Ian Troth, Sarah M. Wallace-Johnson

*Corresponding author. Email: jeam@soton.ac.uk

This PDF file includes:

Supplementary Text
Figs. S1 to S9
Tables S1 to S5
References

Supplementary Text

The geology of the East Greenland Devonian is described in a number of publications (*38, 61-63*) together with detailed reviews (*64, 65*) of the fish and tetrapod localities and their sedimentary environments (*46*). Palynological assemblages through the latest Devonian and Carboniferous sequence have been documented (*14*) but based on a somewhat generalised stratigraphy. However, the D-C boundary can be accurately placed using palynology (*66, 67*). The sequences studied here (fig. S1) included vertical sections (fig. S2) logged in detail through the Celsius Bjerg and Traill Ø (island) Groups from the mountains of Wimans Bjerg, Nathorst Bjerg (*46*) and Stensiö Bjerg on Gauss Halvø, Celsius Bjerg on Ymer Ø, Backlund Ridge on Geographical Society Ø and Rebild Bakker on northern Traill Ø. All the sections (totalling over 1000 m) were directly logged on a 10 cm scale (fig. S2) with particular attention paid to rock color and sediment cycles. Fig. S3 is a full palynological range chart for the Britta Dal to Obrutschew Bjerg Formation interval.

Britta Dal Formation

The Britta Dal Formation (*46*) is a ~460 m interval (Fig. S2) comprises a spectacular cyclic sequence of red, green and purple siltstones. These siltstones are entirely characteristic of vertisols that are arid soils where there was successive seasonal wetting and drying. There are some 196 vertisol cycles present within the Britta Dal and the underlying Wimans Bjerg Formation on Gauss Halvø and, as such, represent a major sustained episode of aridity. No calcrete nodules were found in these siltstones.

Stensiö Bjerg Formation

The Stensiö Bjerg Formation (*46*) is defined by an end to the thick monotonous sequence of Britta Dal Formation vertisols. Instead, there are now palaeosols (aridisols) with calcrete nodules and more rarely individual calcrete beds. There are also numerous fluvial sandstone beds that represent wetter intervals. Also present are rare dark colored, mudstones rich in organic matter that were deposited in stratified permanent lakes when the system became flooded sufficiently to establish perennial lakes. Thus, the prevailing climate of the Stensiö Bjerg Formation was more variable including episodes varying from aridity through to humidity in marked contrast to the sustained aridity of the Britta Dal Formation. Spore assemblages (figs S2, S3) occur beneath the base of the Stensiö Bjerg Formation and their occurrence is coincident with the ending of the sustained aridity that characterises the Britta Dal Formation. The spore assemblage (figs S3, S4) is characterised by locally abundant *Retispora lepidophyta* (sometimes in excess of 60%) and the formation was clearly latest Famennian in age (*68*). The base of the LE spore zone coincides with a lacustrine flooding episode that represents a minor lake within the Stensiö Bjerg Formation but with a maximum TOC of 2.6% that contrasts strongly with the 21% maximum in the overlying Obrutschew Bjerg Formation.

This switch to a climate system with an alternation of more intense arid and humid episodes was coincident with the latest Famennian glaciations in Gondwana as revealed by the range of *Retispora lepidophyta* (*49, 69*).

Obrutschew Bjerg Formation (OBF)

This is the pair of deep permanent stratified lakes that define the D-C boundary and are documented in the main paper. Less well developed lakes within the East Greenland Devonian Basin have depths in excess of 100 m (*70*) so this should be regarded as a minimum for the Obrutschew Formation. Fig. S2 shows a correlation line through 75 km of section with the thin (~4-6 m) Obrutschew Bjerg Formation constrained palynologically in all of these occurrences. Below every occurrence the LN or LN* spore zone can be identified by palynological assemblages that contain many specimens of *Retispora lepidophyta*, the spores *Ancyrospora* and *Hystricosporites* with bifurcate tipped processes, *Diducites* and *Rugospora radiata*. All these spores become extinct at the D-C boundary (6, 10, 69). In the upper part of the Obrutschew Bjerg Formation the palynology assemblage changes to the impoverished VI spore assemblage dominated by simple spores including *Retusotriletes incohatus*, *Plicatispora scolecophora* and *Vallatisporites* that are earliest Tournaisian (Carboniferous) in age.

$\delta^{13}C_{TOC}$ analyses (table S1) were made from the Obrutschew Bjerg Formation samples and this data shows a 9‰ negative shift through the interval. In D-C boundary marine sections (*2*) there is a positive excursion just below the boundary. This 9‰ negative shift from East Greenland is the upper part of this excursion where the value returns to normal and further confirmation of the stratigraphic position.

The Obrutschew Bjerg Formation contains quite a different vertebrate assemblage to the underlying formations as it lacks the otherwise ubiquitous placoderms and contains instead the actinopterygian fish *Cuneognathus* (*71*) in addition to rare predators such as a single shark specimen. No specimens of placoderm or holoptychian fish were found by us above this level despite focused searching on the summits of Stensiö Bjerg, Rebild Bakker and Celsius Bjerg. This level represents the placoderm extinction horizon. Figure S5 I illustrates one of the last holoptychian fish scales to occur within the Stensiö Bjerg Formation.

Harder Bjerg Formation (Traill Ø Group)

This formation has caused much confusion through misidentification (*72*). On the three mountain peaks on Gauss Halvø (fig. S1, blue circles, Stensiö Bjerg, Nathorst Bjerg and Obrutschew Bjerg) there is a very distinctive yellow sandstone of largely aeolian origin (with minor fluvial input) that was deposited above a distinct but subtle angular unconformity surface on very earliest Carboniferous sediments. This is almost certainly the sub-Permian unconformity (*72*) with an overlying 'Rotliegend' equivalent. Failure to recognise this as a significant angular unconformity but instead as a rather minor intra-Carboniferous unconformity, led to the conclusion (*38*) that there was an episode of tectonic deformation immediately above what we can now recognise as the D-C boundary.

It is in the sections on Celsius Bjerg (the Harder Bjerg Formation type section), Backlund Ridge (Geographical Society Ø) and at Rebild Bakker itself (northern Traill Ø) that there is a conformable sequence (largely fluvial sandstone) above the D-C boundary lake. This is genuinely Harder Bjerg Formation and can be palynologically dated (*14*) with contiguous Famennian to Tournaisian to Viséan sections on both Backlund Ridge and Rebild Bakker. In the upper part of the Harder Bjerg Formation on Celsius Bjerg (fig.

S2) there is a second but minor lacustrine interval followed by a further arid episode with vertisols.

The, as yet, unnamed (*14*) formation (fig. S2) above the Harder Bjerg Formation is defined by a return to humid conditions as shown by the occurrence of thin coals, black mudstones with plant fragments, abundant stems and rootlet horizons with trunks, roots and branches of the lycopod *Lepidodendron*. This is coincident with the inception of the *Lepidodendron* spore *Lycospora pusilla* (*14*) and defines the effective base of the Viséan Stage.

International Stratigraphic Correlation of the East Greenland D-C Boundary sections
The key to understanding the D-C boundary extinction event is the time correlation of terrestrial sections from East Greenland with reference marine sections in Europe and the high latitude glacial record from South America. This correlation is achieved using (figs S3, S4) the widely recognised (*69*) extinction of many well-known Devonian spores at the D-C boundary, notably *Retispora lepidophyta* together with all spores with bifurcate sculpture (*Ancyrospora*, *Hystricosporites* and *Nikitinsporites*), *Diducites* spp. and *Rugospora radiata*. All of these spores occur in the lower part of the Obrutschew Bjerg Formation. These extinctions define the LN transitional (or LN*, *10*) to VI spore zone boundary. Immediately below the LN* zone on Stensiö Bjerg there is a red colored interval that includes a 50 cm thick Stage 3 calcrete demonstrating (*47*) an episode of sustained (~25-75 kyr) aridity. Below this there are LE zone spores. Correlation with the base of the LE spore zone from the para-stratotype Stockum II trench section in Germany (*10*) (Fig. 5) demonstrate that this arid interval from Greenland represents the LN spore zone and includes the Hangenberg Black Shale where the marine extinctions are concentrated. This black shale interval is now interpreted (*48*) as the readjustment of the low latitude sedimentary system to glacial driven cooling. This correlates the arid (and cool) interval in East Greenland to the glacial episode.

The correlation can be extended (Fig. 5) to 60° palaeo-south at Chaguaya, Bolivia. Here the D-C boundary can be clearly identified based on significant extinctions in spores and marine phytoplankton including *Retispora lepidophyta* and *Umbellasphaeridium saharicum*. There is also a single specimen high in the section of *Verrucosisporites nitidus* that indicates very latest Devonian although this marker species is not necessarily present in all sections and has been attributed to an ecozone (*27*). However, it is known from other sections in Bolivia (*49, 50*). The Chaguaya section includes a prominent 60-140 m thick interval containing coarse sandstones, striated/grooved hardgrounds and diamictites, which terminates 12 m below the D-C boundary. The unit is traced laterally for >7 km and overlies variably incisive (c. 100 m) relief downcut into shoreface sandstones. It is interpreted to represent successive erosion, proglacial to subglacial deposition, remobilisation, and terminal glacial retreat immediately prior to the D-C boundary. The unit is correlative to regionally developed glacigenic dropstone-in-shale facies (*49*). This places the glacial collapse at the D-C boundary and links it to the terrestrial extinctions.

Forest Collapse at the Devonian-Carboniferous boundary and its impact on the sedimentary environment

The plant specimens plotted on Fig. 2 are stems that were found during a three person traverse on the upper slopes of Celsius Bjerg that was conducted in both uphill and downhill directions on different section lines. Plant specimens were located by GPS including altitude and their width measured by tape measure. The data is on table 2. Following the transect the top of Celsius was searched for a further day and a half and no plants were found above the D-C boundary apart from 4 small specimens in the uppermost (Viséan) levels. Fig. S5 shows a selection of these plant stems that represent the trunks of sizeable trees but were generally preserved as decorticated fragments that lack foliage. They demonstrate the presence of forested areas upstream of the Celsius Bjerg section. Plant stems also occur as rare better preserved compressions (fig. S5 E, F) within the lacustrine sediments of the Obrutschew Bjerg Formation. Coincident with the disappearance of these trunks is the extinction of *Diducites* spp. the spore of *Rhacophyton*, known to be the understory layer (*8*) to the Devonian forests. The response to this loss of both forest and understory cover with the return to the simple VI flora can be observed in the sedimentary environment. Fig. S6 is 50 m of the boundary interval on Celsius Bjerg where the rivers and arid floodplains of the very latest Devonian are replaced by a more fluvial dominated system including gilbert type deltas with thicker sandstones representing a more active fluvial system. The gilbert type deltas typified by highly inclined cross-beds rich in mica flakes formed in a temporary lake as the sedimentary system responded to both the continued more humid conditions of the early Tournaisian and the lack of a structured forest community to slow down the rate of run off. For the first time these channel sandstones carry a bed load of basement clasts (in addition to reworked calcretes) showing these rivers reached to the basin margins. Such basement clasts were absent in the underlying >200 m of latest Famennian section.

Further examples of malformation within Grandispora cornuta

Figs S7 and S8 show many further examples of malformation within *Grandispora cornuta* to emphasise the range of variation in both morphology and darkening.
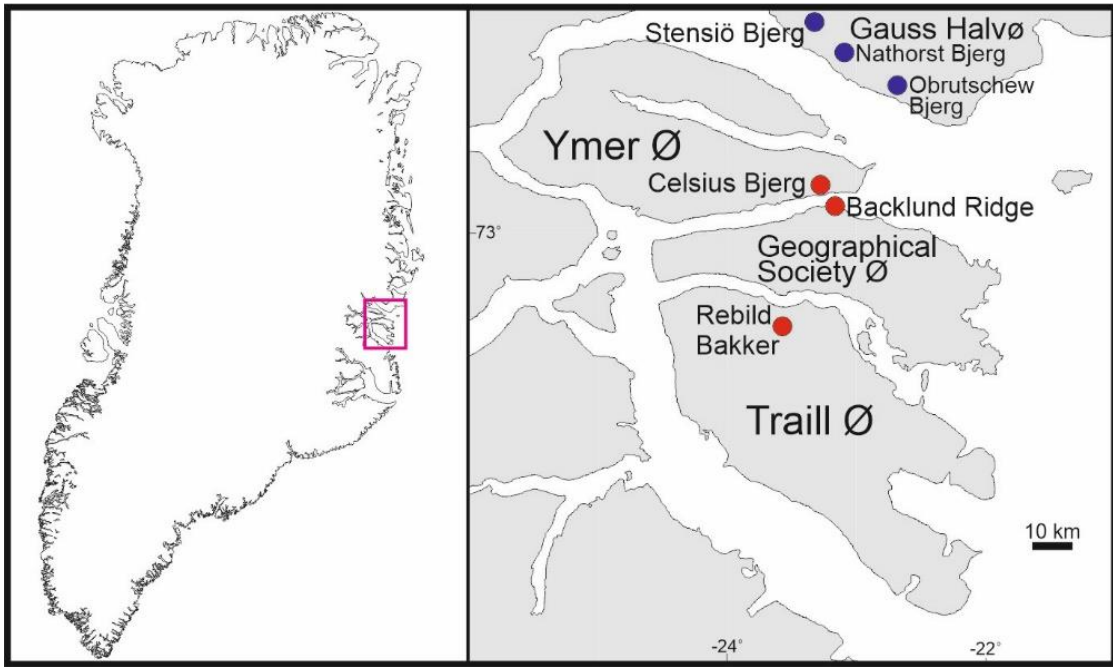
Fig. S1. Location map showing the field sections studied in East Greenland. The blue ● indicates a section where the Obrutschew Bjerg Formation is immediately beneath an unconformity surface. From (*72*)
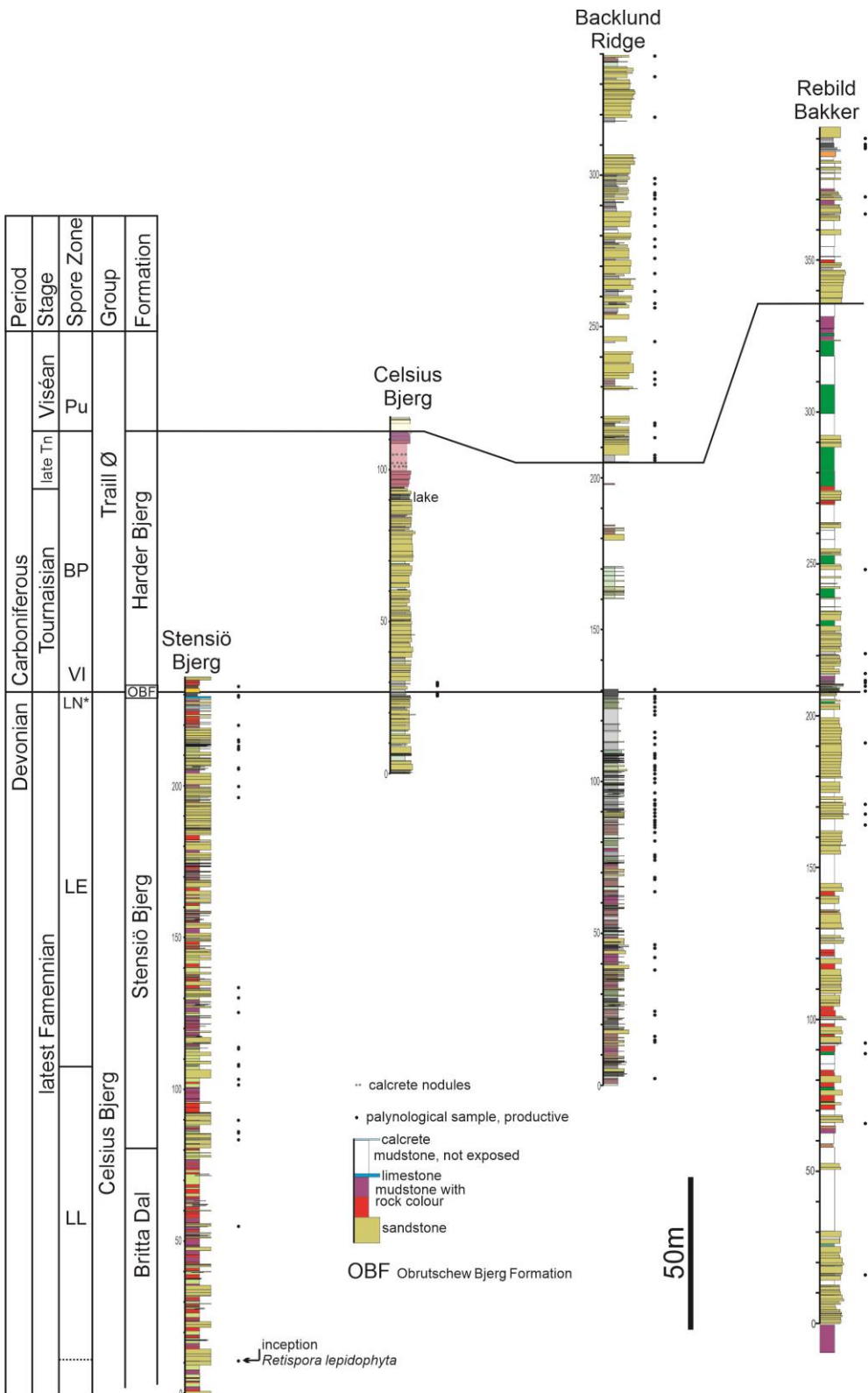
Fig. S2. Correlated fence diagram of East Greenland sections. The LN* to VI spore zone boundary shows that the distinctive lacustrine sediments of the Obrutschew Bjerg Formation (OBF) are coincident with the Devonian-Carboniferous boundary.
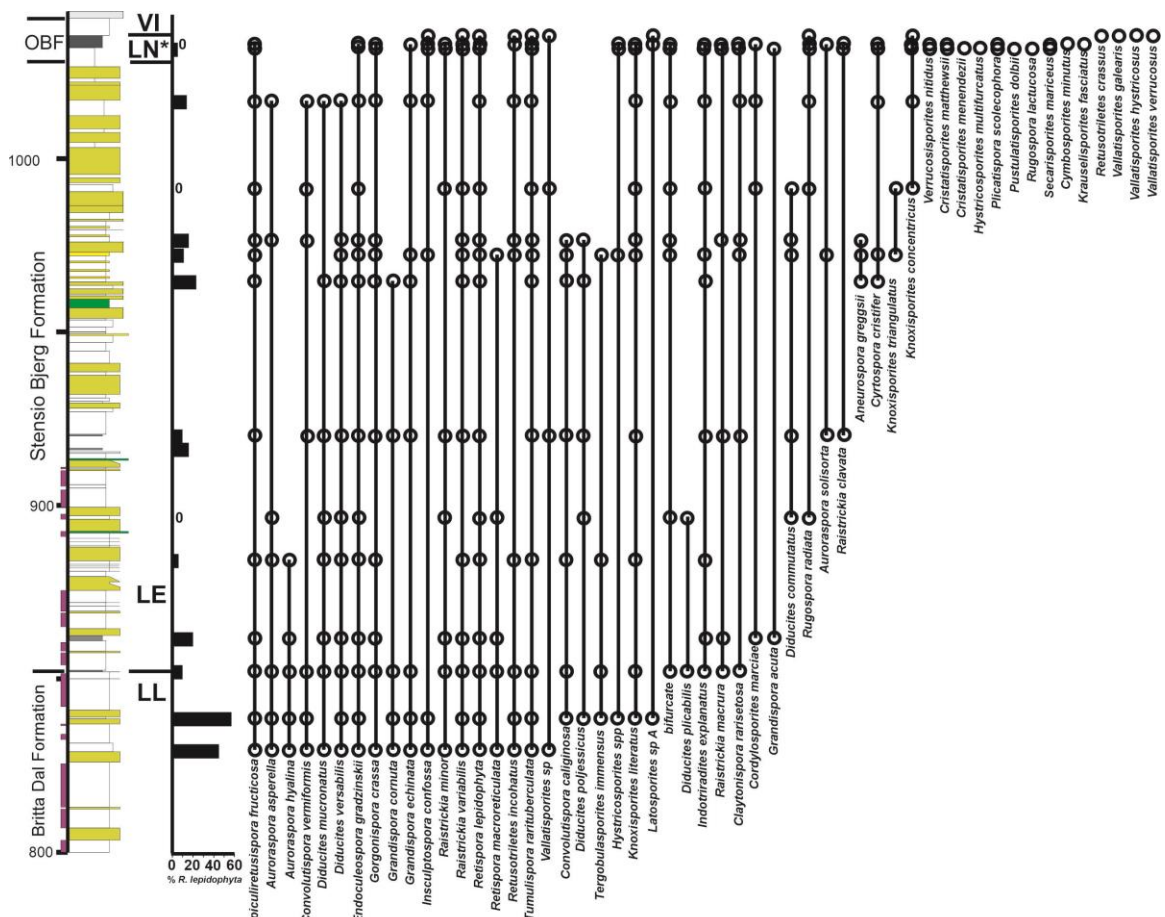
Fig. S3. Full palynological range chart composited from the mountains of Nathorst Bjerg and Stensiö Bjerg showing details of the assemblage, the evidence for palynological zonation and the relative abundance of *Retispora lepidophyta*. OBF is the Obrutschew Bjerg Formation. Sedimentary log from (46).
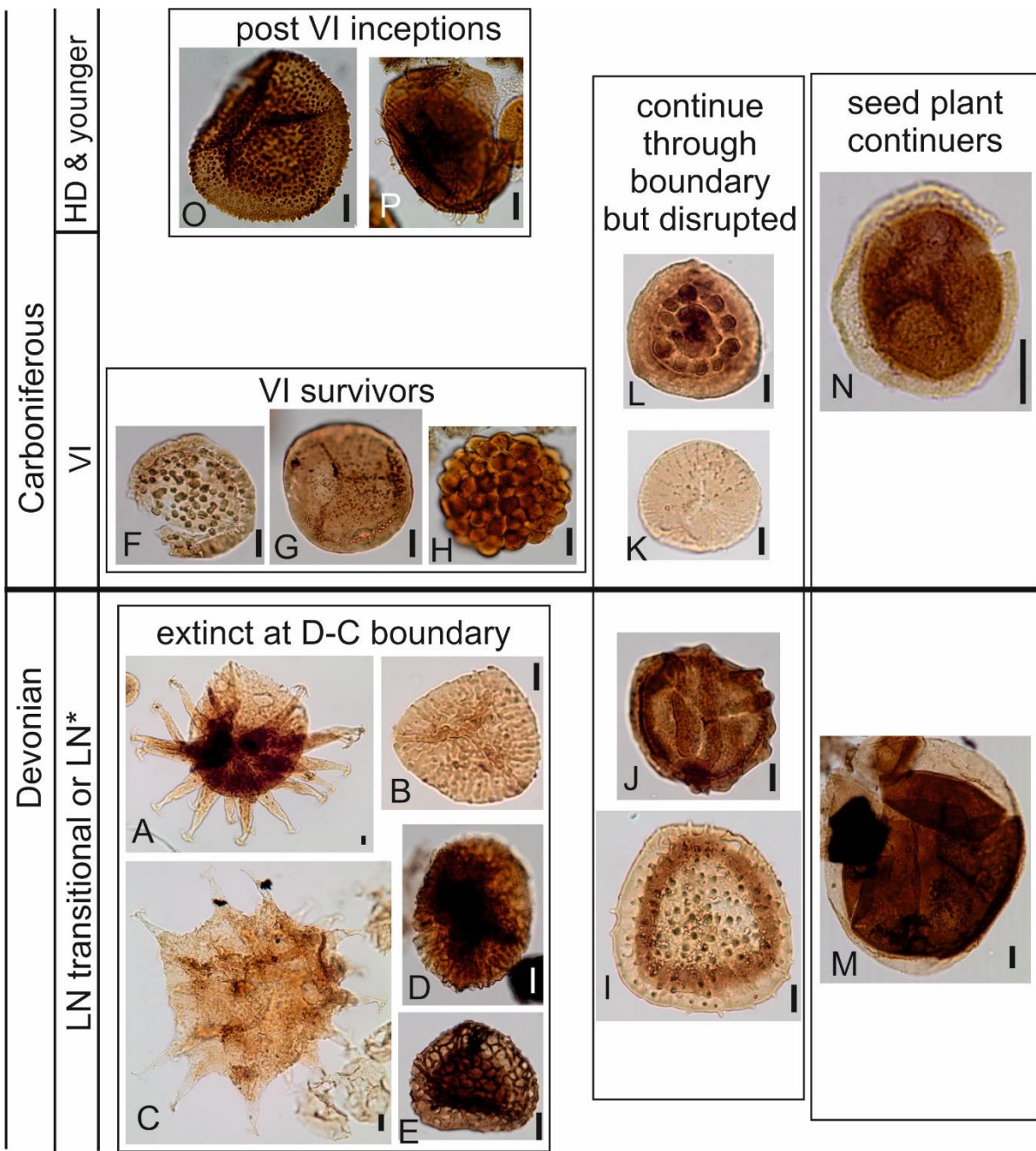
Fig. S4. Examples of important spores and pollen from the D-C boundary sections in East Greenland and their relationship to the boundary. **A**. *Hystricosporites* sp. **B**. *Rugospora radiata* **C**. *Ancyrospora capillata* **D**. *Diducites variabilis* **E**. *Retispora lepidophyta* **F**. *Vallatisporites verrucosus* **G**. *Retusotriletes incohatus* **H**. *Verrucosisporites nitidus* **I**. *Indotriradites explanatus* **J**. *Knoxisporites concentricus* **K**. *Claytonispora rarisetosa* **L**. *Tumulispora rarituberculata* **M**. *Remysporites/Velamisporites* **N**. *Auroraspora asperella* **O**. *Spelaeotriletes obtusus* **P**. *Claytonispora distincta*. All scale bars 10 μm. Sample and slide numbers plus England Finder co-ordinates are on table S4.

Fig. S5. Representatives of the plant stems measured on the traverse of specimens across the D-C boundary on Celsius Bjerg. The stems are normally decorticated. The spiral arrangement on **C** is typical of a lycopod. **D** is a trunk base. **E** and **F** (the latter is a part and counter-part) are better preserved compressions from the lower part of the Obrutschew Bjerg Formation. **H** is a branching stem. **I** is one of the last holoptychian fish scales found in the Devonian 4.5 m below base of the Obrutschew Bjerg Formation. All scale bars 10 cm, except **E** and **I** that are 2.5 cm. Photo credit: John Marshall, University of Southampton.
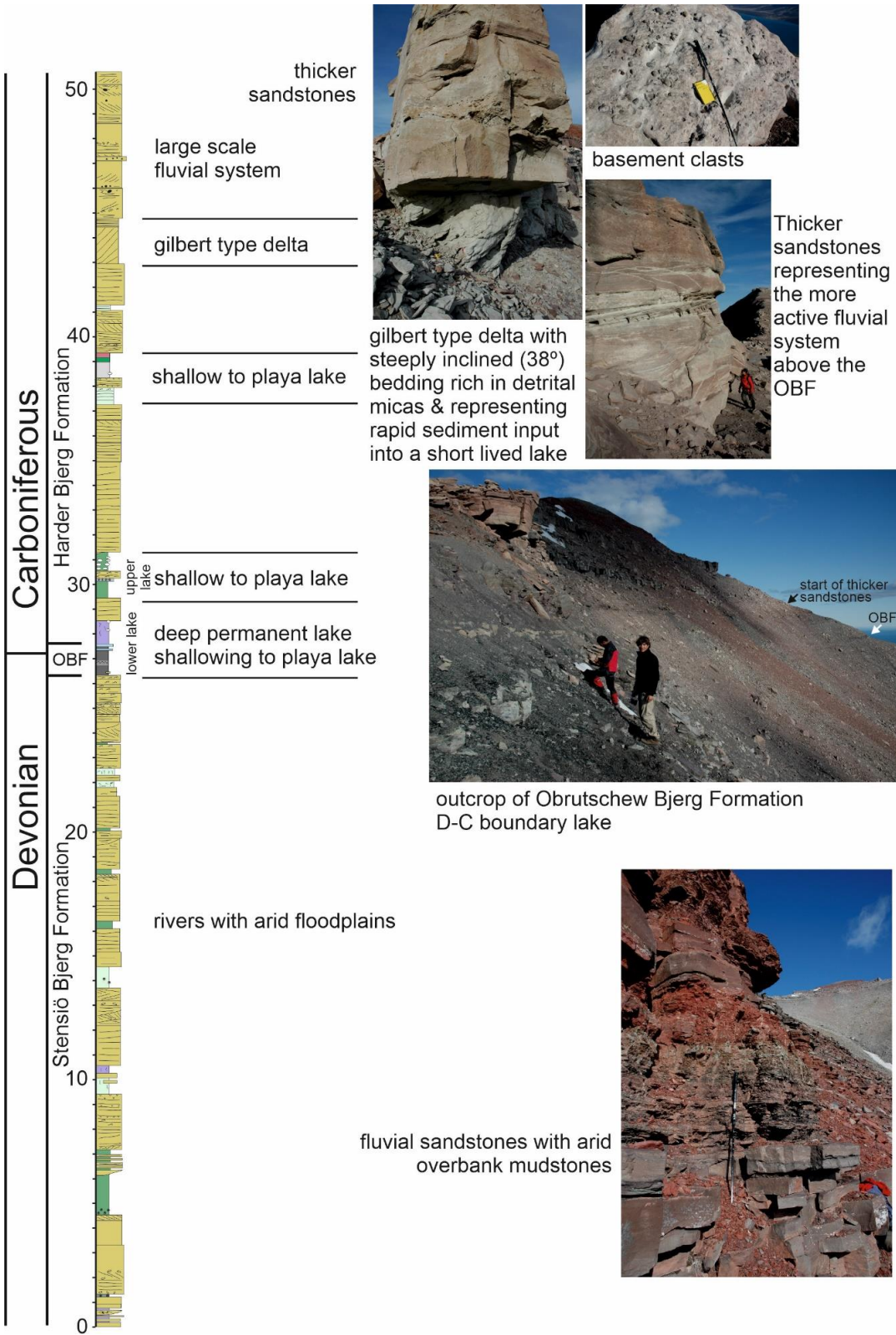
Fig. S6. The D-C boundary interval on Celsius Bjerg showing representative sedimentary environments and the change to larger more extensive fluvial systems following collapse of the terrestrial environment. Photo credit: John Marshall, University of Southampton.
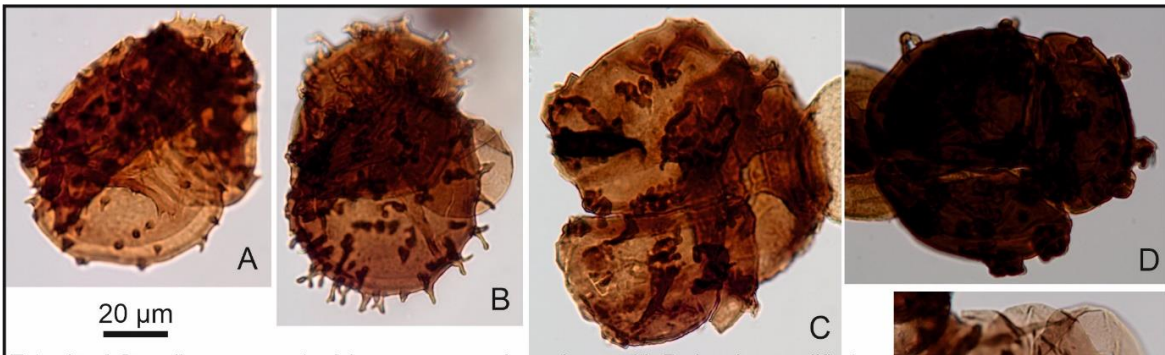
Tetrads of *Grandispora cornuta*. A is a near normal specimen with B showing modified sculpture and an inner body without the external wall layer but part of the tetrad. In C the sculpture is reduced to irregular sporopollenin masses. D has very irregular sculpture and the specimen is very dark. E is a tetrad of inner bodies without any outer wall layers.
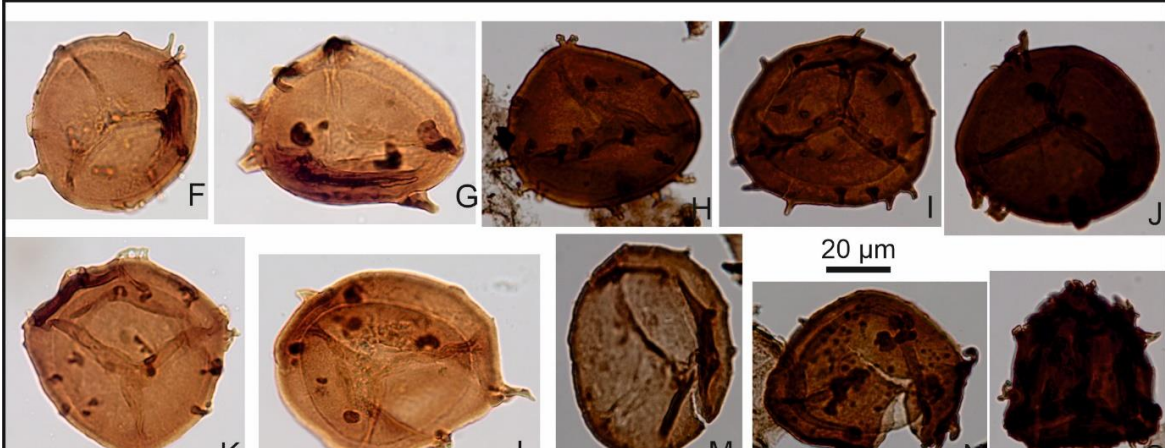
Malformed specimens of *Grandispora cornuta* with irregularly spaced sculpture. This sculpture ranges from robust spines (F), to irregular masses (O), hooked tips, coalesced adjacent spines (K) and specimens largely devoid of spines (M). There is a range of darkening shown by individual specimens.
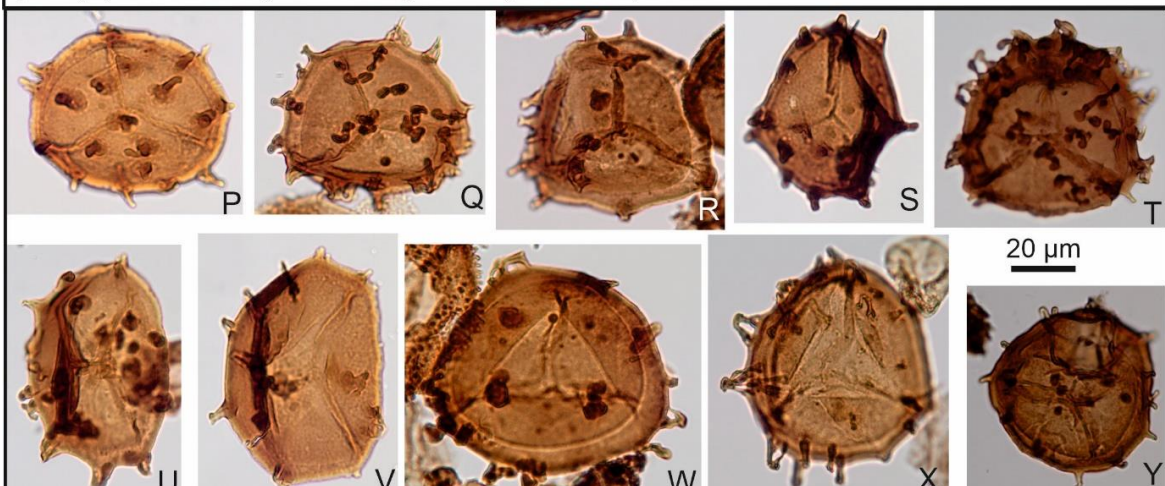
A range of malformed specimens of *Grandispora cornuta* with broad spines with generally blunt tips that can also become hooked (Y, W), coalesced (T, X) or reduced to irregular masses. The spacing is often irregular (R) and there can be a range of spine types on single specimens (R, W). A range of darkening is present.

**Fig. S7** shows many further examples of malformation within *Grandispora cornuta* to emphasise the range of variation in both morphology and darkening. Sample and slide numbers plus England Finder co-ordinates are on table S4.
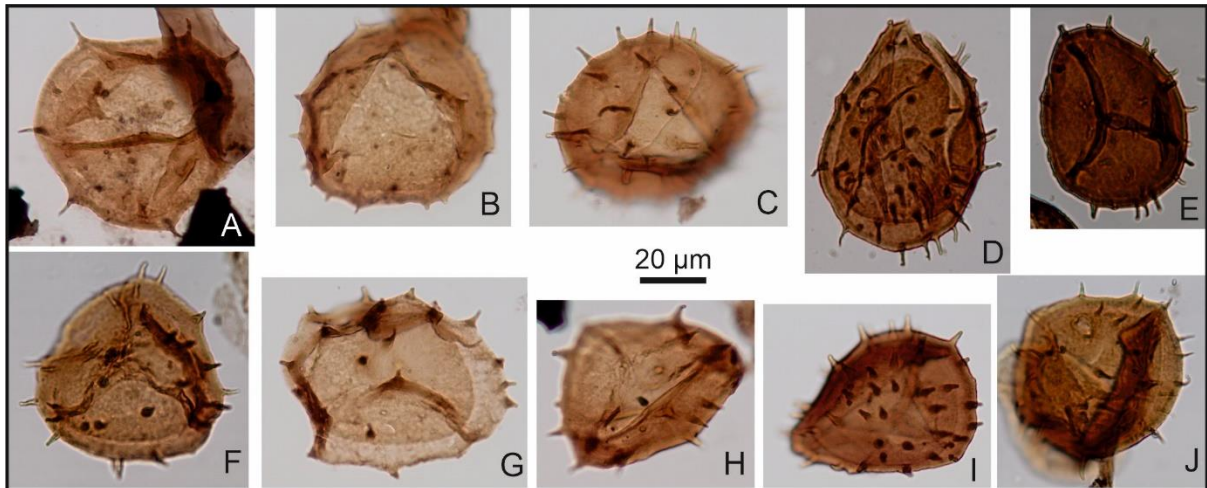
Malformed *Grandispora cornuta* with pointed spines and which are close to normal forms (A) but with variability in spine spacing (G), spine length (B), thickness (I) and degree of darkening
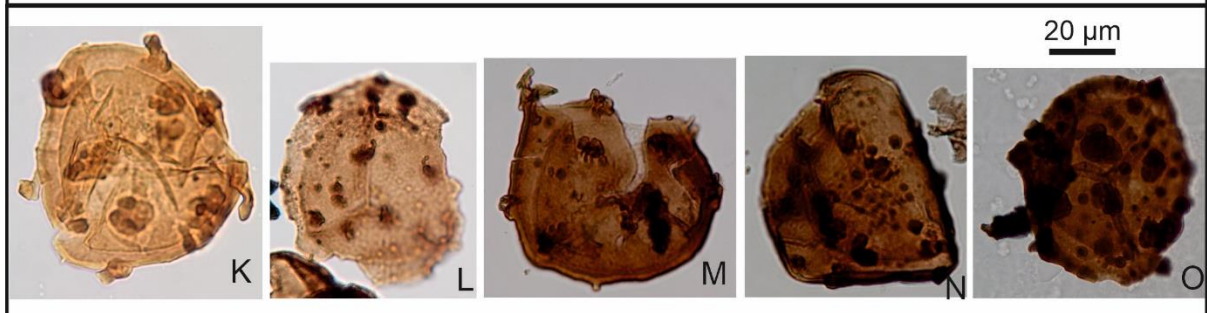
Malformed *Grandispora cornuta* with residual sculpture deposited as irregular lumps of sporopollenin. The spore bodies also show a variety of malformations in shape and degree of sporopollenisation of the walls. Again there is a range of wall darkening.

Fig. S8 shows many further examples of malformation within *Grandispora cornuta* to emphasize the range of variation in both morphology and darkening. Sample and slide numbers plus England Finder co-ordinates are on table S4.
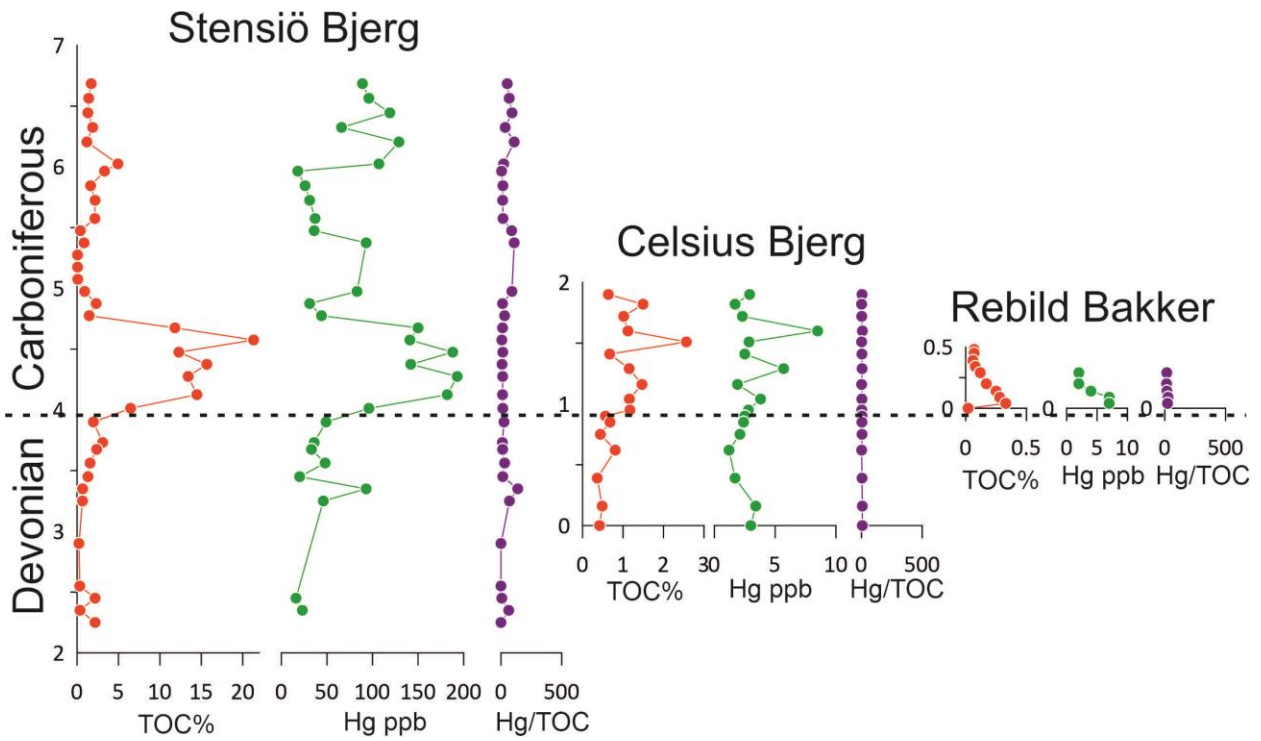
Fig. S9. TOC% and mercury (Hg) data from Stensio Bjerg, Celsius Bjerg and Rebild Bakker. Any LIP related source of Hg will be shown by an anomalous Hg/TOC value. At mass extinction levels with known LIP involvement Hg/TOC anomalies are generally in the 1000s (*73*). In all three sections, including Rebild Bakker with direct evidence of a kill mechanism, the maximum Hg/TOC is 138 with an average of 26 and median of 14. Hg/TOC is scaled here as 0-500 to be comparable to a LIP profile.

Stensiö Bjerg height (m)	sample	TOC%	calcite%	Hg ppb	Hg/TOC	δ¹³C_TOC	
						$\delta^{13}C_{TOC}$	
6.69	Sten 52	1.71	12	89	52	-28.35	upper sample, Fig. 1
6.57	Sten 51	1.41	12	96	68	-28.24	
6.45	Sten 50	1.31	10	119	91	-28.18	
6.33	Sten 49	1.89	5	66	35	-29.48	
6.21	Sten 48	1.19	20	129	109	-29.64	
6.03	Sten 47	4.94	9	107	22	-30.98	
5.97	Sten 46	3.32	12	18	5	-31.01	
5.85	Sten 45	1.64	11	26	16	-30.05	
5.73	Sten 44	2.18	10	31	14	-30.15	
5.58	Sten 43	2.16	8	37	17	-30.10	
5.48	Sten 42	0.41	13	36	88	-26.27	
5.38	Sten 41	0.85	0	93	109	-29.94	
5.28	Sten 40	0.06	16				
5.18	Sten 39	0.07	18				
5.08	Sten 38	0.09	20				
4.98	Sten 37	0.92	24	83	90	-27.91	
4.88	Sten 36	2.31	36	31	13	-27.94	
4.78	Sten 35	1.47	24	44	30	-27.98	
4.68	Sten 34	11.82	0	150	13	-28.82	
4.58	Sten 33	21.32	0	141	7	-29.17	
4.48	Sten 32	12.29	0	188	15	-29.21	
4.38	Sten 31	15.67	0	142	9	-28.50	
4.28	Sten 30	13.42	0	193	14	-28.85	
4.13	Sten 29	14.47	0	182	13	-29.47	
4.01	Sten 28	6.47	19	96	15	-29.91	
3.90	Sten 27	1.98	9	49	25	-24.82	
3.73	Sten 26	3.09	16	36	12	-27.77	
3.68	Sten 25	2.37	25	33	14	-27.20	
3.56	Sten 24	1.58	29	48	30	-27.04	
3.45	Sten 23.5	1.32	35	20	15	-26.39	
3.35	Ob 8	0.67	39	93	138	-25.05	
3.25	Ob 7	0.66	41	46	70	-24.54	
2.90	Ob 5	0.23	39		0	-22.11	
2.55	Ob 4	0.33	38		0	-24.11	
2.45	Ob 3	2.18	15	16	7	-25.82	
2.35	Ob 2	0.36	40	23	64	-23.59	
2.25	Ob 1	2.18	34		0	-27.19	lowest sample, Fig. 1

Table S1. Analytical data and sample numbers/heights from the Stensiö Bjerg Devonian-Carboniferous boundary. Total and acidified carbon analyzed were reproportioned as per (*74*)

altitude (m)	stem width (cm)																
1247	1	1	1	2													
1099-1239	0																
1089	10																
1079	4																
1077	5																
1072	2																
1067	5	3	4														
1065	8	5	3														
1061	6	6															
1035	4	8	3	4	3	6											
1032	8																
1024	5	4	5	6													
1020	2	10	3														
1015	9	3															
1012	3																
1010	2																
1003	1																
997	10																
992	13	4															
988	4																
980	0																
974	4																
947	10																
939	6																
927	3	1	2	4	2	1	4	1	7	8	3	2	3	3	3		
924	7																
922	3																
917	6																
911	2	4	4	4	1	1	2	2	3	2	2	5	3	2	6	5	2
911	2	3	4	10	9	6	6	4	1	7	1	5	7	1	1	20	14
911	3	4	1	6	6	3	9	2	3	2	4	1	5	4	4	2	3
906	6																
902	2	6	5	4													
900	2																
898	1																
896	5	3															
893	4	3	2														
892	1	0	1	3	4	1											
891	6																
890	5																
888	3																
887	2																
878	3																
874	4																
865	6	2	8														
861	3																
856	5																

Table S2. Abundance, stem width and distribution of plant stems on Celsius Bjerg below and above the Devonian-Carboniferous boundary. Heights are by GPS altimeter.

Rebild Bakker, lower lake

height (m)	sample	TOC%	calcite%	Hg ppb	Hg/TOC		count of *Grandispora cornuta*					Translucency			
							malformed	normal	tetrads	total		min	max	mean	stdev
0.48	RB-17-17	0.07	16												
0.45	RB-17-16	0.07	9												
0.39	RB-17-15	0.06	11												
0.34	RB-17-14	0.08	10												
0.29	RB-17-13	0.12	13	2	16		130	5	2	137		6.5	30.3	15.1	6.0
0.20	RB-17-12	0.17	12	2	14		110	1	20	131		8.7	50.5	21.9	8.8
0.14	RB-17-11	0.25	12	4	17		101	3	13	117		10.8	59.6	30.9	13.8
0.09	RB-17-10	0.28	13	7	26		95	10	14	119		15.6	68.4	44.1	14.1
0.04	RB-17-9	0.33	6	7	22		82	26	8	116		18.1	77.3	46.7	12.1
0.00	RB-17-8B	0.02	11												

Celsius, lower lake

height (m)	sample	TOC	calcite	Hg ppb	Hg/TOC
1.90	CEL-18	0.64	51	3	4.5
1.82	CEL-17	1.49	39	2	1.1
1.72	CEL-16	1.02	64	2	2.3
1.60	CEL-15	1.12	22	9	7.6
1.51	CEL-14	2.56	36	3	1.1
1.41	CEL-13	0.67	38	3	3.7
1.29	CEL-12	1.15	11	6	4.9
1.16	CEL-11	1.47	22	2	1.3
1.04	CEL-10	1.16	23	4	3.3
0.95	CEL-9	1.17	20	3	2.4
0.90	CEL-8	0.57	35	3	4.4
0.85	CEL-7	0.68	21	2	3.5
0.75	CEL-6	0.44	23	2	4.8
0.62	CEL-5	0.81	22	1	1.5
0.39	CEL-4	0.36	19	2	4.7
0.16	CEL-3	0.49	16	3	7.0
0.00	CEL-2	0.42	12	3	7.1

Vitrinite reflectivity from Viséan coal, RB17-37

UTM 27X 0411062 8077299 789m, 173 m above lower lake

Rv	count	st dev	min	max
0.70	72	0.072	0.58	0.83

Table S3. Analytical data and sample numbers/heights from the Rebild Bakker and Celsius Bjerg Devonian-Carboniferous boundary section together with the vitrinite reflectivity data from a Viséan coal on Rebild Bakker. Vitrinite to temperature conversion was using (*75*)

Fig. 3		sample	x	y	EF	Fig. S7		sample	x	y	EF
Grandispora cornuta	D	RB-17 12(lc)	122.1	15.9	M21/2	*Grandispora cornuta*	A	RB17-12 (xm)	127.4	20.2	G27/3
Grandispora cornuta	E	RB17-11	119.1	10.6	R18/4	*Grandispora cornuta*	B	RB17-12 (xm)	135.7	15.4	M35/4
Grandispora cornuta	F	RB17-12 (3)	117.1	11.2	R16/2	*Grandispora cornuta*	C	RB17-12 (xm)	138.0	11.2	R38/1
Grandispora cornuta	G	RB17-12	130.3	8.1	U30/1	*Grandispora cornuta*	D	RB17-12	120.0	20.6	G19/2
Grandispora cornuta	H	RB17-12 (3)	121.7	8.7	T21/3	*Grandispora cornuta*	E	RB17-13	124.1	8.4	U23/2
Grandispora cornuta	I	RB17-12	124.5	11.0	R24/1	*Grandispora cornuta*	F	RB17-12 (xm)	120.8	12.1	Q20/2
Grandispora cornuta	J	RB17-12	122.4	16.4	L22/3	*Grandispora cornuta*	G	RB17-12 (xm)	121.3	10.9	R20/2
Grandispora cornuta	K	RB17-9	122.3	11.0	R22/1	*Grandispora cornuta*	H	RB17-12	123.8	10.6	R23/4
Grandispora cornuta	L	RB17-12	136.7	6.1	W36/2	*Grandispora cornuta*	I	RB17-12	131.7	10.6	R31/4
Grandispora cornuta	M	RB17-12 (3)	127.1	21.7	F27/1	*Grandispora cornuta*	J	RB17-12	126.0	4.8	X25/4
Grandispora cornuta	N	RB17-12 (sq)	132.0	12.2	Q32/1	*Grandispora cornuta*	K	RB17-12 (xm)	133.4	8.2	U23/1
Grandispora cornuta	O	RB17-12	142.1	6.0	W42	*Grandispora cornuta*	L	RB17-12 (xm)	141.2	21.2	F41/4
Grandispora cornuta	P	RB17-12 (3)	129.2	7.6	U29/3	*Grandispora cornuta*	M	RB17-12	125.0	19.4	H24/4
Grandispora cornuta	Q	RB17-12	124.5	8.2	U24/1	*Grandispora cornuta*	N	RB17-12	122.5	17.7	K22/1
Grandispora cornuta	R	RB17-12	127.0	10.0	S26/2	*Grandispora cornuta*	O	RB17-12	130.3	7.8	U30/3
Grandispora cornuta	S	RB17-12	122.1	6.0	W21/2	*Grandispora cornuta*	P	RB17-12 (xm)	129.7	14.2	N29/4
Grandispora cornuta	T	RB17-12 (3)	121.3	17.2	K21/3	*Grandispora cornuta*	Q	RB17-12 (xm)	115.5	11.3	R14/2
Grandispora cornuta	U	RB17-9	114.7	11.4	Q14/3	*Grandispora cornuta*	R	RB17-12 (xm)	120.0	14.9	N19/2
Grandispora cornuta	V	RB17-13 (4)	134.0	5.0	X34/1	*Grandispora cornuta*	S	RB17-12 (xm)	127.2	12.2	Q27/1
Grandispora cornuta	W	RB17-12	141.0	20.5	G41/3	*Grandispora cornuta*	T	RB17-12 (3)	131.9	7.2	V31/2
						Grandispora cornuta	U	RB17-12 (xm)	135.6	22.1	E35/4
Fig. 4						*Grandispora cornuta*	V	RB17-12 (xm)	112.8	9.3	T12/1
Verrucosisporites nitidus	A	Sten 23.5	144.0	12.6	P44/4	*Grandispora cornuta*	W	RB17-12 (xm)	138.0	10.0	S38/3
Verrucosisporites nitidus	B	Sten 23.5	140.9	14.8	N41/3	*Grandispora cornuta*	X	RB17-12 (xm)	114.5	6.2	W13/2
Verrucosisporites nitidus	C	Sten 23.5	146.2	12.4	P46/4	*Grandispora cornuta*	Y	RB17-12	117.3	20.5	G16/2
Verrucosisporites nitidus	D	RB17-10 (1)	132.0	19.3	H32/3						
Verrucosisporites nitidus	E	RB17-12 (2)	126.0	17.1	L25/2	**Fig. S8**					
Verrucosisporites nitidus	F	RB17-12 (3)	133.7	4.2	Y33/2	*Grandispora cornuta*	A	RB17-10 (1)	119.0	11.2	R18/2
Verrucosisporites nitidus	G	RB17-12 (3)	135.8	10.8	R35/4	*Grandispora cornuta*	B	RB17-10 (1)	119.0	9.2	T18/2
Verrucosisporites nitidus	H	RB17-9	127.7	4.7	X27/4	*Grandispora cornuta*	C	RB17-10 (1)	127.1	12.0	Q27/1
Verrucosisporites nitidus	I	RB17-12 (3)	130.6	6.8	V30/3	*Grandispora cornuta*	D	RB17-12	134.2	5.1	X34/1
Verrucosisporites nitidus	J	RB17-11 (1)	120.4	6.1	W20/1	*Grandispora cornuta*	E	RB17-12	123.7	8.7	T23/3
Verrucosisporites nitidus	K	RB17-10 (2)	136.6	13.2	P36/2	*Grandispora cornuta*	F	RB17-11 (1)	127.6	15.0	N27/2
Verrucosisporites nitidus	L	RB17-10	118.6	21.1	F18/3	*Grandispora cornuta*	G	RB17-10 (1)	122.0	9.1	T21/2
Verrucosisporites nitidus	M	RB17-11	130.8	3.6	Y30/4	*Grandispora cornuta*	H	RB17-11 (2)	113.0	13.0	P12/1
Verrucosisporites nitidus	N	RB17-48(us)	131.9	11.0	R31/2	*Grandispora cornuta*	I	RB17-12 (3)	124.3	7.6	U23/4
Verrucosisporites nitidus	O	RB17-48(us)	131.0	11.0	R31/1	*Grandispora cornuta*	J	RB17-11	123.8	16.6	L23/4
Verrucosisporites nitidus	P	RB17-49(1)	127.7	15.2	N27/2	*Grandispora cornuta*	K	RB17-12 (xm)	137.6	19.0	J37/2
						Grandispora cornuta	L	RB17-12 (xm)	121.9	10.8	R21/3
Fig. S4						*Grandispora cornuta*	M	RB17-12	121.8	17.2	K21/3
Hystricosporites sp	A	M5744	129.9	10.0	S29/2	*Grandispora cornuta*	N	RB17-2	116.5	10.9	R16/1
Rugospora radiata	B	M5743	117.7	17.2	L17/1	*Grandispora cornuta*	O	RB17-11 (1)	137.1	3.9	Y37/3
Ancyrospora capillata	C	OB7	129.5	13.9	O29/2						
Diducites variabilis	D	RB17-43	137.1	4.5	Y37/1						
Retispora lepidophyta	E	RB17-43	137.4	5.8	W37/4						
Vallatisporites verrucosus	F	Sten 43	129.5	6.1	W29/2						
Retusotriletes incohatus	G	Sten 43	126.8	11.8	Q26/2						
Verrucosisporites nitidus	H	RB17-49 (1)	127.7	15.2	M27/4						
Indotriradites explanatus	I	M5744	124.8	20.7	G24/2						
Knoxisporites concentricus	J	M5743	116.8	17.1	L16/1						
Claytonispora rarisetosa	K	M5744	117.4	15.1	N17/1						
Tumulispora malevkensis	L	M5744	116.0	14.2	O15/2						
Remysporites magnificus	M	RB17-11 (1)	114.3	15.4	M13/4						
Auroraspora asperella	N	RB17-11 (1)	114.3	16.4	L13/4						
Spelaeotriletes obscurus	O	Rebild 14 (1)	134.0	11.8	Q34/3						
Claytonispora distincta	P	Rebild 14 (1)	135.0	12.7	P35/3						

Table S4. Sample numbers and slide co-ordinates for spores illustrated on Figs 3 and 4 and figs S4, S7 and S8.

RB-17-46A		RB-17-9		RB-17-10		RB-17-11		RB-17-12		RB-17-13		RB-17-19		RB-17-20		RB-17-48		RB-17-50	
0.62	1.33	0.41	2.23	0.48	1.73	0.57	1.86	0.46	1.54	0.38	1.69	0.37	1.27	0.64	2.24	0.31	1.19	0.24	1.55
0.66	1.33	0.47	2.23	0.60	1.74	0.63	1.87	0.48	1.57	0.53	1.70	0.48	1.74	0.68	2.25	0.41	1.20	0.26	1.61
0.70	1.33	0.47	2.25	0.61	1.74	0.66	1.87	0.62	1.62	0.82	1.70	0.50	1.86	0.75	2.25	0.42	1.33	0.26	1.68
0.71	1.34	0.61	2.29	0.66	1.75	0.68	1.88	0.62	1.62	0.85	1.72	0.52	1.87	0.76	2.26	0.43	1.34	0.37	1.68
0.73	1.35	0.68	2.36	0.67	1.79	0.78	1.89	0.65	1.62	0.88	1.72	0.53	2.12	0.81	2.29	0.46	1.44	0.38	1.69
0.74	1.35	0.70	2.38	0.79	1.80	0.81	1.91	0.67	1.62	0.94	1.76	0.56	2.15	0.83	2.37	0.49	1.45	0.39	1.74
0.76	1.35	0.70	2.46	0.81	1.81	0.87	1.91	0.67	1.62	0.97	1.76	0.64	2.27	0.97	2.38	0.49	1.52	0.42	1.83
0.78	1.36	0.80	2.52	0.81	1.88	0.88	1.93	0.70	1.62	0.98	1.76	0.65	2.46	0.97	2.41	0.50	1.59	0.45	2.08
0.82	1.37	0.82	2.70	0.90	1.89	0.88	1.94	0.70	1.63	1.02	1.81	0.66	2.63	1.00	2.44	0.50	1.65	0.51	2.13
0.84	1.37	0.84	2.72	0.91	1.92	0.88	1.95	0.71	1.68	1.11	1.82	0.67	2.65	1.00	2.51	0.51	1.73	0.51	2.20
0.85	1.38	0.88	2.73	0.93	1.93	0.89	1.97	0.72	1.70	1.11	1.86	0.69	2.80	1.03	2.52	0.53	1.74	0.51	2.23
0.85	1.40	0.90	2.75	0.94	1.96	0.91	1.97	0.76	1.70	1.13	1.86	0.70	2.84	1.03	2.56	0.54	1.74	0.54	2.26
0.85	1.41	0.91	2.82	0.97	1.96	0.92	1.98	0.79	1.74	1.14	1.86	0.71	2.98	1.06	2.60	0.56	1.77	0.54	2.27
0.86	1.41	0.91	2.82	0.99	1.97	1.00	1.99	0.81	1.75	1.15	1.90	0.71	3.01	1.12	2.68	0.57	1.78	0.54	2.29
0.86	1.44	0.92	2.94	1.03	1.98	1.04	1.99	0.87	1.79	1.15	1.91	0.73	3.05	1.15	2.81	0.57	1.79	0.57	2.29
0.88	1.44	0.92	2.95	1.03	2.00	1.07	2.04	0.89	1.79	1.16	1.92	0.75	3.10	1.29	2.82	0.57	1.80	0.60	2.35
0.88	1.45	0.96	3.02	1.04	2.01	1.12	2.04	0.92	1.79	1.16	1.93	0.78	3.18	1.30	2.83	0.60	1.90	0.60	2.35
0.91	1.45	0.99	3.07	1.04	2.01	1.19	2.05	0.93	1.79	1.17	1.94	0.80	3.22	1.31	2.86	0.61	1.90	0.62	2.37
0.94	1.46	1.01	3.07	1.11	2.01	1.24	2.05	0.95	1.81	1.18	1.95	0.81	3.23	1.34	2.94	0.67	1.95	0.63	2.40
0.95	1.46	1.02	3.19	1.11	2.05	1.29	2.05	0.95	1.84	1.19	1.98	0.82	3.27	1.34	2.96	0.67	1.96	0.64	2.48
0.97	1.48	1.19	3.27	1.19	2.05	1.29	2.06	0.96	1.85	1.23	1.99	0.82	3.27	1.35	3.02	0.70	1.99	0.67	2.60
0.97	1.53	1.20	3.33	1.24	2.06	1.36	2.07	1.01	1.86	1.23	2.01	0.82	3.28	1.39	3.06	0.70	2.03	0.67	2.65
0.99	1.54	1.23	3.40	1.25	2.09	1.37	2.09	1.01	1.92	1.25	2.03	0.83	3.36	1.43	3.08	0.70	2.08	0.70	2.80
1.00	1.54	1.26	3.46	1.28	2.10	1.41	2.11	1.04	1.92	1.27	2.07	0.84	3.43	1.46	3.11	0.70	2.12	0.70	2.88
1.01	1.54	1.28	3.56	1.28	2.11	1.41	2.12	1.05	1.93	1.27	2.11	0.85	3.45	1.49	3.12	0.71	2.16	0.73	2.90
1.02	1.57	1.30	3.68	1.30	2.11	1.42	2.15	1.06	1.96	1.28	2.25	0.85	3.46	1.51	3.15	0.73	2.23	0.82	2.96
1.02	1.58	1.32	3.69	1.30	2.16	1.44	2.17	1.07	1.98	1.31	2.38	0.85	3.48	1.52	3.16	0.74	2.26	0.82	3.00
1.03	1.58	1.33	3.79	1.32	2.16	1.44	2.19	1.08	2.00	1.31	2.41	0.86	3.50	1.55	3.19	0.76	2.31	0.84	3.04
1.04	1.58	1.35	3.88	1.32	2.17	1.44	2.26	1.15	2.01	1.31	2.48	0.86	3.60	1.58	3.21	0.77	2.38	0.88	3.10
1.04	1.59	1.44	3.90	1.34	2.18	1.47	2.28	1.19	2.03	1.32	2.52	0.86	3.65	1.58	3.21	0.77	2.40	0.90	3.13
1.07	1.59	1.46	3.98	1.35	2.21	1.49	2.29	1.22	2.05	1.34	2.59	0.86	3.66	1.61	3.31	0.78	2.43	0.91	3.15
1.07	1.60	1.57	4.02	1.36	2.30	1.52	2.29	1.23	2.09	1.34	2.61	0.86	3.69	1.64	3.33	0.80	2.47	0.95	3.24
1.10	1.60	1.60	4.15	1.37	2.33	1.56	2.32	1.26	2.11	1.36	2.62	0.88	3.70	1.69	3.39	0.80	2.48	0.97	3.26
1.11	1.68	1.60	4.19	1.39	2.36	1.57	2.33	1.27	2.24	1.36	2.64	0.89	3.76	1.82	3.44	0.81	2.51	1.08	3.29
1.12	1.72	1.64	4.28	1.40	2.40	1.59	2.37	1.27	2.48	1.37	2.67	0.90	3.91	1.84	3.45	0.83	2.64	1.12	3.36
1.13	1.73	1.65	4.30	1.41	2.42	1.60	2.45	1.30	2.62	1.37	2.68	0.92	3.92	1.85	3.46	0.86	2.81	1.22	3.43
1.14	1.74	1.66	4.30	1.42	2.50	1.60	2.49	1.33	2.62	1.39	2.70	0.93	3.93	1.88	3.48	0.87	2.94	1.22	3.47
1.15	1.75	1.67	4.32	1.45	2.50	1.61	2.58	1.36	2.74	1.39	2.70	0.96	4.01	1.89	3.54	0.88	2.95	1.22	3.51
1.20	1.76	1.68	4.35	1.47	2.66	1.62	2.63	1.38	2.93	1.40	2.71	0.96	4.03	1.92	3.54	0.89	3.04	1.30	3.52
1.23	1.86	1.70	4.47	1.50	2.67	1.66	2.64	1.38	2.98	1.41	2.81	1.04	4.12	1.94	3.77	0.89	3.23	1.30	3.59
1.23	1.87	1.72	4.61	1.50	2.69	1.66	2.73	1.43	3.01	1.42	2.98	1.04	4.20	1.96	3.88	0.91	3.40	1.37	3.67
1.25	1.95	1.76	4.63	1.52	2.80	1.68	2.84	1.43	3.06	1.50	3.38	1.04	4.24	1.99	3.93	0.91	3.48	1.40	3.71
1.26	1.96	1.77	4.76	1.55	2.85	1.77	3.26	1.44	3.37	1.52	3.42	1.06	4.48	2.02	3.94	0.95	3.51	1.40	3.78
1.26	1.98	1.77	4.86	1.57	2.88	1.78	3.35	1.45	3.39	1.56	3.57	1.06	4.66	2.03	3.95	0.97	3.51	1.44	4.01
1.27	1.98	1.79	4.87	1.58	3.01	1.82	3.45	1.45	3.63	1.60	3.62	1.17	4.71	2.05	3.96	1.07	3.62	1.47	4.16
1.30	2.11	1.84	4.93	1.60	3.20	1.83	3.53	1.46	3.69	1.62	3.63	1.19	4.80	2.07	4.08	1.08	3.77	1.47	4.26
1.30	2.13	1.95	4.97	1.66	3.52	1.83	3.86	1.47	3.70	1.63	3.75	1.19	4.85	2.08	4.11	1.08	3.90	1.48	4.29
1.31	2.16	2.05	5.44	1.68	3.66	1.84	4.50	1.51	3.79	1.63	4.18	1.19	5.09	2.12	4.50	1.09	4.19	1.48	4.40
1.32	2.20	2.12	5.55	1.71	4.00	1.85	4.50	1.53	4.04	1.64	4.18	1.22	5.20	2.21	4.79	1.12	4.27	1.50	4.42
1.32	2.57	2.22	5.20	1.72	4.05	1.85	4.93	1.54	4.92	1.68	4.36	1.24	5.25	2.21	5.22	1.19	4.29	1.54	4.53

Table S5. Phytoclast reflectivity data from the lower and upper lakes, Rebild Bakker section showing presence of charcoal across the Devonian-Carboniferous boundary. Charcoal definition after (*76*), measurements made from polished thins (*77*).

REFERENCES AND NOTES

1. P. M. Myrow, J. Ramezani, A. E. Hanson, S. A. Bowring, G. Racki, M. Rakociński, High-precision U-Pb age and duration of the latest Devonian (Famennian) Hangenberg event, and its implications. *Terra Nova* **26**, 222–229 (2013).

2. S. I. Kaiser, M. Aretz, R. T. Becker, The global Hangenberg Crisis (Devonian-Carboniferous transition): Review of a first-order mass extinction. *Geol. Soc. Lond. Spec. Pub.* **423**, 387–437 (2016).

3. D. P. G. Bond, S. E. Grasby, On the causes of mass extinction. *Palaeogeogr. Palaeoclimatol. Palaeoecol.* **478**, 3–29 (2017).

4. L. C. Sallan, M. I. Coates, End-Devonian extinction and a bottleneck in the early evolution of modern jawed vertebrates. *Proc. Natl. Acad. Sci. U.S.A.* **107**, 10131–10135 (2010).

5. D. Silvestro, B. Cascales-Miñana, C. D. Bacon, A. Antonelli, Revisiting the origin and diversification of vascular plants through a comprehensive Bayesian analysis of the fossil record. *New Phytol.* **207**, 425–436 (2015).

6. K. Higgs, G. Clayton, J. B. Keegan, Stratigraphic and systematic palynology of the Tournaisian Rocks of Ireland. *Geol. Surv. Ireland Spec. Pap.* **7**, 1–93 (1988).

7. P. M. Van Veen, Aspects of late Devonian and early Carboniferous palynology of Southern Ireland. V. The change in composition of palynological assemblages at the Devonian-Carboniferous boundary. *Rev. Palaeobot. Palynol.* **34**, 67–97 (1981).

8. S. F. Greb, W. A. DiMichele, R. A. Gastaldo, Evolution and importance of wetlands in earth history. *Geol. Soc. Am. Spec. Pap.* **399**, 1–40 (2006).

9. J. P. Benca, I. A. P. Duijnstee, C. V. Looy, UV-B–induced forest sterility: Implications of ozone shield failure in Earth's largest extinction. *Sci. Adv.* **4**, e1700618 (2018).

10. K. T. Higgs, M. Streel, D. Korn, E. Paproth, Palynological data from the Devonian-Carboniferous boundary beds in the new Stockum Trench II and the Hasselbachtal borehole, Northern Rhenish Massif, Germany. *Ann. Soc. Geol. Belg.* **115**, 551–557 (1993).

11. M. Streel, S. E. Scheckler, Miospore lateral distribution in upper Famennian alluvial lagoonal to tidal facies from eastern United States and Belgium. *Rev. Palaeobot. Palynol.* **64**, 315–324 (1990).

12. F. M. Gradstein, J. G. Ogg, M. Schmitz, G. Ogg, *Geological Time Scale* (Elsevier, 2020).

13. A.-L. Decombeix, B. Meyer-Berthaud, J. Galtier, Transitional changes in arborescent lignophytes at the Devonian-Carboniferous boundary. *J. Geol. Soc. Lond.* **168**, 547–557 (2011).

14. J. O. Vigran, L. Stemmerik, S. Piasecki, Stratigraphy and depositional evolution of the uppermost Devonian-Carboniferous (Tournaisian- Westphalian) non-marine deposits in North-East Greenland. *Palynology* **23**, 115–152 (1999).

15. K. T. Higgs, C. Prestianni, M. Streel, J. Thorez, High resolution miospore stratigraphy of the Upper Famennian of eastern Belgium, and correlation with the conodont zonation. *Geol. Belg.* **16**, 84–94 (2013).

16. E. Turnau, V. I. Avchimovitch, T. V. Byvscheva, G. Clayton, K. T. Higgs, B. Owens, Taxonomy and stratigraphical distribution of *Verrucosisporites nitidus* Playford, 1964 and related species. *Rev. Palaeobot. Palynol.* **81**, 289–295 (1994).

17. B. R. Murphy, F. J. G. Mitchell, An association between past levels of ozone column depletion and abnormal pollen morphology in the model angiosperm *Arabidopsis thaliana* L. *Rev. Palaeobot. Palynol.* **194**, 12–20 (2013).

18. C. B. Foster, S. A. Afonin, Abnormal pollen grains: An outcome of deteriorating atmospheric conditions around the Permian-Triassic boundary. *J. Geol. Soc. Lond.* **162**, 653–659 (2005).

19. R. Hopkins, How ultraviolet light reacts in cells (2015); https://www.nature.com/scitable/blog/scibytes/how_ultraviolet_light_reacts_in.

20. K. Mičieta, G. Murín, Three species of genus Pinus suitable as bioindicators of polluted environment. *Water Air Soil Pollut.* **104**, 413–422 (1998).

21. H. Visscher, C. V. Looy, M. E. Collinson, H. Brinkhuis, J. H. A. van Konijnenburg-van Cittert, W. M. Kürchner, M. A. Sephton, Environmental mutagenesis during the end-Permian ecological crisis. *Proc. Natl. Acad. Sci. U.S.A.* **101**, 12952–12956 (2004).

22. P. A. Hochuli, E. Schneebell-Hermann, G. Mangerud, H. Bucher, Evidence for atmospheric pollution across the Permian-Triassic transition. *Geology* **45**, 1123–1126 (2017).

23. B. van der Schootbrugge, T. M. Quan, S. Lindström, W. Püttmann, C. Heunisch, J. Pross, J. Fiebig, R. Petschick, H.-G. Röhling, S. Richoz, Y. Rosenthal, P. G. Falkowski, Floral changes across the Triassic/Jurassic boundary linked to flood basalt volcanism. *Nat. Geosci.* **2**, 589–594 (2009).

24. S. Lindström, H. Sanei, B. van de Schootbrugge, G. K. Pedersen, C. E. Lesher, C. Tegner, C. Heunisch, K. Dybkjær, P. M. Outridge, Volcanic mercury and mutagenesis in land plants during the end-Triassic mass extinction. *Sci. Adv.* **5**, eaaw4018 (2019).

25. J. R. Flenley, Why is pollen yellow? And why are there so many species in the tropical rain forest? *J. Biogeogr.* **38**, 809–816 (2011).

26. P. Filipiak, G. Racki, Proliferation of abnormal palynoflora during the end-Devonian biotic crisis. *Geol. Quart.* **54**, 1–14 (2010).

27. C. Prestianni, M. Sautois, J. Denayer, Disrupted continental environments around the Devonian Carboniferous Boundary: Introduction of the *tener* event. *Geol. Belg.* **19**, 135–145 (2016).

28. L. M. E. Percival, H. C. Jenkyns, T. A. Mather, A. J. Dickson, S. J. Batenburg, M. Ruhl, S. P. Hesselbo, R. Barclay, I. Jarvis, S. A. Robinson, L. Woelders, Does large igneous province volcanism always perturb the mercury cycle? Comparing the records of Oceanic Anoxic Event 2 and the end-Cretaceous to other Mesozoic events. *Am. J. Sci.* **318**, 799–860 (2018).

29. D. P. G. Bond, P. B. Wignall, *Large igneous provinces and mass extinctions: An update*. GSA Spec. Pap. **505**, 29–55 (2014).

30. R. E. Ernst, S. A. Rodygin, O. M. Grinev, Age correlation of Large Igneous Provinces with Devonian biotic crises. *Global Planet. Change* **185**, 103097 (2020).

31. O. Paschall, S. K. Carmichael, P. Königshof, J. A. Waters, P. H. Ta, T. Komatsu, A. Dombrowski, The Devonian-Carboniferous boundary in Vietnam: Sustained ocean anoxia with a volcanic trigger for the Hangenberg Crisis?. *Global Planet. Change* **175**, 64–81 (2019).

32. H. Sanei, P. M. Outridge, A. Dallimore, P. B. Hamilton, Mercury-organic matter relationships in pre-pollution sediments of thermokarst lakes from the Mackenzie River Delta, Canada: The role of depositional environment. *Biogeochemistry* **107**, 149–164 (2012).

33. J. Kalvoda, T. Kumpan, W. Qie, J. Frýda, O. Bábek, Mercury spikes at the Devonian-Carboniferous boundary in the eastern part of the Rhenohercynian Zone (central Europe) and in the South China Block. *Palaeogeogr. Palaeoclimatol. Palaeoecol.* **531**, 109221 (2019).

34. P. Ward, C. Labandeira, M. Laurin, R. A. Berner, Confirmation of Romer's Gap as a low oxygen interval constraining the timing of initial arthropod and vertebrate terrestrialization. *Proc. Natl. Acad. Sci. U.S.A.* **103**, 16818–16822 (2006).

35. J. A. Clack, C. E. Bennett, D. K. Carpenter, S. J. Davies, N. C. Fraser, T. I. Kearsey, J. E. A. Marshall, D. Millward, B. K. A. Otoo, E. J. Reeves, A. J. Ross, M. Ruta, K. Z. Smithson, T. R. Smithson, S. A. Walsh, Phylogenetic and environmental context of a Tournaisian tetrapod fauna. *Nat. Ecol. Evol.* **1**, 0002 (2016).

36. S. R. Schachat, C. C. Labandeira, M. R. Saltzman, B. D. Cramer, J. L. Payne, C. K. Boyce, Phanerozoic pO_2 and the early evolution of terrestrial animals. *Proc. R. Soc. B* **285**, 20172631 (2018).

37. C. M. Belcher, J. M. Yearsley, R. M. Hadden, J. C. McElwain, G. Rein, Baseline intrinsic flammability of Earth's ecosystems estimated from paleoatmospheric oxygen over the past 350 million years. *Proc. Natl. Acad. Sci. U.S.A.* **107**, 22448–22453 (2010).

38. H. Olsen, Sedimentary basin analysis of the continental Devonian basin in North-East Greenland. *Bull. Grønlands Geol. Unders.* **168**, 1–80 (1993).

39. T. H. Torsvik, L. R. M. Cocks, *Earth History and Palaeogeography* (Cambridge Univ. Press, 2017).

40. W. Ehrmann, G. Schmeidel, S. Beuscher, S. Krüger, Intensity of African humid periods estimated from Saharan dust fluxes. *PLOS ONE* **12** e0170989 (2017).

41. T. Vollmer, R. Wemer, M. Weber, N. Tougiannidis, H.-G. Röhling, U. Hambach, Orbital control on Upper Triassic playa cycles of the Steinmergel-Keuper (Norian): A new concept for ancient playa cycles. *Palaeogeogr. Palaeoclimatol. Palaeoecol.* **267**, 1–16 (2008).

42. H. Olsen, Orbital forcing on continental depositional systems—Lacustrine and fluvial cyclicity in the Devonian of East Greenland. *Spec. Publs Int. Ass. Sediment.* **19**, 429–438 (1994).

43. J. G. Anderson, D. M. Wilmouth, J. B. Smith, D. S. Sayres, UV dosage levels in summer: Increased risk of ozone loss from convectively injected water vapour. *Science* **337**, 835–839 (2012).

44. M. L. Caplan, R. M. Bustin, Devonian-Carboniferous Hangenberg mass extinction event, widespread organic-rich mudrock and anoxia: Causes and consequences. *Palaeogeogr. Palaeoclimatol. Palaeoecol.* **148**, 187–207 (1999).

45. M. G. Scarratt, R. M. Moore, Production of methyl bromide and methyl chloride in laboratory cultures of marine phytoplankton II. *Mar. Chem.* **59**, 311–320 (1998).

46. T. R. Astin, J. E. A. Marshall, H. Blom, C. M. Berry, The sedimentary environment of the Late Devonian East Greenland tetrapods. *Geol. Soc. Lond. Spec. Pub.* **339**, 93–109 (2010).

47. G. J. Retallack, *A Colour Guide To Paleosols* (Wiley, 1997).

48. O. J. Bábek, T. Kumpan, J. Kalvoda, T. M. Grygar, Devonian/Carboniferous boundary glacioeustatic fluctuations in a platform-to-basin direction: A geochemical approach of sequence stratigraphy in pelagic settings. *Sed. Geol.* **337**, 81–99 (2016).

49. R. Wicander, G. Clayton, J. E. A. Marshall, I. Troth, A. Racey, Was the latest Devonian glaciation a multiple event? New palynological evidence from Bolivia. *Palaeogeogr. Palaeoclimatol. Palaeoecol.* **305**, 75–83 (2011).

50. P. E. Isaacson, E. Díaz-Martinez, G. W. Grader, J. Kalvoda, O. Babek, F. X. Devuyst, Late Devonian-earliest Mississippian glaciation in Gondwanaland and its biogeographic consequences, *Palaeogeogr. Palaeoclimatol. Palaeoecol.* **268**, 126–142 (2008).

51. J. A. Lakin, J. E. A. Marshall, I. Troth, I. C. Harding, Greenhouse to icehouse: A biostratigraphic review of latest Devonian–Mississippian glaciations and their global effects. *Geol. Soc. Lond. Spec. Pub.* **423**, 439–464 (2016).

52. D. K. Brezinski, C. B. Cecil, V. W. Skema, Late Devonian glacigenic and associated facies from the central Appalachian Basin, eastern United States. *GSA Bull.* **122**, 265–281 (2010).

53. F. R. Ettensohn, J. C. Pashin, W. Gilliam, The Appalachian and Black Warrior Basins: Foreland basins in the eastern United States, in *The Sedimentary Basins of the United States and Canada*, A. D. Miall, Ed. (Elsevier, ed. 2, 2019), pp. 129–237.

54. D. Edwards, M. Fairon-Demaret, C. M. Berry, Plant megafossils in Devonian stratigraphy: A progress report. *Cour. Forsch.-Inst. Senckenberg* **220**, 25–37 (2000).

55. M. Friedman, L. C. Sallan, Five hundred million years of extinction and recovery: A Phanerozoic survey of large-scale diversity patterns in fishes. *Palaeontology* **55**, 707–742 (2012).

56. T. R. Smithson, S. P. Wood, J. E. A. Marshall, J. A. Clack, Earliest Carboniferous tetrapod and arthropod faunas from Scotland populate Romer's Gap. *Proc. Natl. Acad. Sci. U.S.A.* **109**, 4532–4537 (2012).

57. S. I. Kaiser, T. Kumpan, M. W. Rasser, High-resolution conodont biostratigraphy in two key sections from the Carnic Alps (Grüne Schneid) and Graz Paleozoic (Trolp)—Implications for the biozonation concept at the Devonian-Carboniferous boundary. *Newsl. Stratigr.* (2020).

58. E. M. Fleischmann, The measurement and penetration of ultraviolet radiation into tropical marine water. *Limnol. Oceanogr.* **34**, 1623–1629 (1989).

59. S. M. Starnes, C. A. Kennedy, J. W. Petranka, Sensitivity of embryos of southern Appalachian amphibians to ambient solar UV-B radiation. *Conserv. Biol.* **14**, 277–282 (2000).

60. L. W. Alvarez, W. Alvarez, F. Asaro, H. V. Michel, Extraterrestrial cause for the Cretaceous-Tertiary extinction, *Science*, **208**, 1095–1108 (1980).

61. H. Olsen, P.-H. Larsen, Lithostratigraphy of the continental Devonian sediments in North-East Greenland. *Geol. Surv. Den. Greenl.* **165**, 1–108 (1993).

62. N. Henriksen, *Geological History Of Greenland* (GEUS, Denmark, 2008).

63. P.-H. Larsen, H. Olsen, J. A. Clack, The Devonian basin in East Greenland—Review of basin evolution and vertebrate assemblages. *GSA Memoir* **202**, 273–292 (2008).

64. H. Blom, J. A. Clack, P. E. Ahlberg, M. Friedman, Devonian vertebrates from East Greenland: A review of faunal composition and distribution. *Geodiversitas* **29**, 119–141 (2007).

65. H. Blom, J. A. Clack, P. E. Ahlberg, Localities, distribution and stratigraphical context of the Late Devonian tetrapods of East Greenland. *Medd. Grønl. Geosci.* **43**, 1–50 (2005).

66. J. E. A. Marshall, T. R. Astin, J. A. Clack, The East Greenland tetrapods are Devonian in age. *Geology* **27**, 637–640 (1999).

67. M. Streel, J. E. A. Marshall, Devonian-Carboniferous boundary global correlations and their paleogeographic implications for assembly of Pangaea. *Proc. XVth Int. Cong. Carb. Perm. Strat.* **2006**, 481–496 (2006).

68. N. Maziane, K. T. Higgs, M. Streel, Biometry and paleoenvironment of *Retispora lepidophyta* (Kedo)Playford 1976 and associated miospores in the latest Famennian nearshore marine facies, eastern Ardenne (Belgium). *Rev. Palaeobot. Palynol.* **118**, 211–226 (2002).

69. M. Streel, K. Higgs, S. Loboziak, W. Riegel, P. Steemans, Spore stratigraphy and correlation with faunas and floras in the type marine Devonian of the Ardenne-Rhenish regions. *Rev. Palaeobot. Palynol.* **50**, 211–229 (1987).

70. J. E. A. Marshall, B. J. Stephenson, Sedimentological responses to basin initiation in the Devonian of East Greenland. *Sedimentology* **44**, 407–419 (1997).

71. M. Friedman, H. Blom, A new actinopterygian fish from the Famennian of East Greenland and the interrelationships of Devonian ray-finned fishes. *J. Paleont.* **80**, 1186–1204 (2006).

72. J. E. A. Marshall, K. W. Glennie, T. R. Astin, A. J. Hewett, The Old Red Group (Devonian) – Rotliegend (Permian) Unconformity in the Inner Moray Firth. *Geol. Soc. Lond. Spec. Pub.* **471**, 237–252 (2019).

73. J. Shen, J. Chen, T. J. Algeo, S. Yuan, Q. Feng, J. Yu, L. Zhou, B. O'Connell, N. J. Planavsky, Evidence for a prolonged Permian-Triassic extinction interval from global marine mercury records. *Nat. Commun.* **10**, 1563 (2019).

74. H. S. Morgans-Bell, A. L. Coe, S. P. Hesselbo, H. C. Jenkyns, G. P. Weedon, J. E. A. Marshall, R. V. Tyson, C. J. Williams, Integrated stratigraphy of the Kimmeridge Clay Formation (Upper Jurassic) based on exposures and boreholes in south Dorset, UK. *Geol. Mag.* **138**, 511–539 (2001).

75. C. E. Barker, M. J. Pawlewicz, Calculation of vitrinite reflectance from thermal histories and peak temperatures: A comparison of methods. *ACS Symp. Ser. Am. Chem. Soc.* **570**, 216–229 (1994).

76. A. C. Scott, I. J. Glasspool, Observations and experiments on the origin and formation on the inertinite group macerals. *Int. J. Coal Geol.* **70**, 53–66 (2007).

77. S. Hillier, J. E. A. Marshall, A rapid technique to make polished thin sections of sedimentary organic matter concentrates. *J. Sediment. Res.* **58**, 754–755 (1988).